Nuclear Materials and Energy 20 (2019) 100691

Contents lists available at ScienceDirect

Nuclear Materials and Energy

journal homepage: www.elsevier.com/locate/nme

Effects of gas puff and pump on plasma detachment associated with molecular activated recombination in GAMMA 10/PDX

Kunpei Nojiri*, Mizuki Sakamoto, Naomichi Ezumi, Akihiro Terakado, Takaaki Iijima, Satoshi Togo, Takayuki Yokodo, Yosuke Kinoshita, Tomohiro Mikami, Tsubasa Yoshimoto, Sotaro Yamashita, Junko Kohagura, Masayuki Yoshikawa, Yousuke Nakashima

Plasma Research Center, University of Tsukuba, 1-1-1 Tennodai, Tsukuba 305-8577, Japan

ARTICLE INFO

Keywords:
Plasma detachment
Molecular activated recombination (MAR)
Pumping
Hydrogen molecule

ABSTRACT

Gas puff and pump experiments on the plasma applied in a divertor simulation were conducted in the GAMMA 10/PDX tandem mirror. Additional hydrogen gas was supplied to the plasma with and without a pump in the region of the divertor simulation. To decrease the electron temperature near the target plate, the gas is supplied at a higher plenum pressure with the use of a pump than without a pump. We observed differences in the characteristics of the plasma detachment caused by molecular activated recombination (MAR) between cases with and without a pump at the same electron temperature. Near the target plate, particle loss with the use of a pump is smaller than that without a pump. By contrast, the vibrational and rotational temperatures of hydrogen molecules in the two cases are almost identical. The density of hydrogen molecules with a pump is lower than that without a pump, indicating that the electron temperature can be decreased even with a lower hydrogen density when a pump is applied. These results suggest that one of reasons for the suppression of the MAR with the use of a pump is the low density of the hydrogen molecules.

1. Introduction

Divertor detachment resulting from plasma–gas interactions is considered an effective method to reduce the heat and particle load on the divertor plates in magnetic confinement fusion devices. Thus far, this has been achieved by increasing the plasma density in the core or by seeding an additional neutral gas in the divertor plasma in torus devices [1–4]. Because atomic and molecular processes play an important role in the detachment, the characteristics of plasma detachment depend on the parameters of not only charged particles but also of neutral atoms and molecules. Regarding the atomic effect, it has been experimentally suggested that atoms in the scrape-off layer (SOL) and divertor region have energy obtained from the plasma and that the density must be higher than that of the neutral atoms at rest to decrease the plasma pressure and achieve detachment [5]. An important phenomenon related to the molecular effects is molecular activated recombination (MAR). The MAR is a volumetric recombination associated with vibrationally and rotationally excited molecules, and has a higher rate coefficient than electron-ion recombination (EIR) at a relatively higher electron temperature (T_e) [6,7]. Linear devices [8] have contributed significantly to an experimental understanding of MAR, including an observation of its first evidence [9], an observation of its reaction chains such as a dissociative attachment (DA) followed by a mutual neutralization (MN) of negative and plasma ions [10], and an observation of the presence of triatomic molecular ions [11] produced through an ion conversion between molecules and diatomic molecular ions (MIC). Theoretically, the cross-section and rate coefficient of the MAR processes change by some orders of magnitude with the vibrational and rotational states of hydrogen molecules [12,13]. Another fundamental study has shown theoretically that the neutral transport lowers the density of H_2 under a high vibrational state and the reaction rate of MAR [14]. It is therefore important to investigate the effects of neutral parameters, as well as the electron temperature (T_e) and ion temperature (T_i), on plasma detachment.

* Corresponding author.
E-mail addresses: nojiri_kunpei@prc.tsukuba.ac.jp (K. Nojiri), sakamoto@prc.tsukuba.ac.jp (M. Sakamoto), ezumi@prc.tsukuba.ac.jp (N. Ezumi), terakado_akihiro@prc.tsukuba.ac.jp (A. Terakado), iijima@prc.tsukuba.ac.jp (T. Iijima), togo@prc.tsukuba.ac.jp (S. Togo), yokodo_takayuki@prc.tsukuba.ac.jp (T. Yokodo), kinoshita_yosuke@prc.tsukuba.ac.jp (Y. Kinoshita), mikami_tomohiro@prc.tsukuba.ac.jp (T. Mikami), yoshimoto_tsubasa@prc.tsukuba.ac.jp (T. Yoshimoto), yamashita_sotaro@prc.tsukuba.ac.jp (S. Yamashita), kohagura@prc.tsukuba.ac.jp (J. Kohagura), yosikawa@prc.tsukuba.ac.jp (M. Yoshikawa), nakashma@prc.tsukuba.ac.jp (Y. Nakashima).

https://doi.org/10.1016/j.nme.2019.100691
Received 15 August 2018; Received in revised form 31 May 2019; Accepted 4 June 2019
Available online 05 June 2019

Divertor simulation experiments have been carried out in the GAMMA 10/PDX tandem mirror using the end-loss plasma, which has a high T_i for studying the characteristics of the detached plasma [15–17]. The plasma detachment associated with MAR has been observed when additional H_2 gas is supplied to the divertor simulation plasma, and the characteristics of the detached plasma have been studied [17–19]. Based on electron parameters such as T_e and the density (n_e), as well as the hydrogen Balmer line intensities, it has been suggested that the detachment is caused by the mutual neutralization of H^- and H^+ following a dissociative attachment enhanced by a dissociative recombination of H^{3+} [17]. Spatial distributions of the above parameters indicate that the MAR processes are enhanced near the target plate [18,19].

The aim of this study is to investigate the neutral particle effect on the plasma detachment associated with MAR in GAMMA 10/PDX. To change the neutral parameters, we conducted a new approach using the combination of a gas puff and pump utilizing the strong pumping system of GAMMA 10/PDX. In the present paper, the effects of the gas puff and pump on the plasma detachment associated with MAR are discussed.

2. Experiment setup

Fig. 1(a) shows a schematic view of a half body (west side) of the GAMMA 10/PDX tandem mirror, which is composed of a central cell, anchor cells, barrier cells, plug cells, and end regions. The length of the device is 27 m and the volume of the vacuum vessel is 150 m^3. In the west end region, the divertor simulation experimental module (D-module) is installed. Fig. 1(b) shows a schematic view of the D-module, which consists of a stainless-steel cuboid chamber with an inlet hole and a V-shaped target. The vertical position of the D-module can be changed. When the D-module is fixed along the Z-axis of GAMMA 10/PDX, the plasma that exits from the mirror confinement regions (i.e., end-loss plasma) flows toward the target plate in the D-module. The size of the chamber is 480 mm × 500 mm × 700 mm for the X- Y-, and Z-directions. The size of each side of the V-shaped target is 300 mm × 350 mm. Tungsten plates with a thickness of 0.2 mm are attached to the target base. The open angle of the V-shaped target can be changed, and was 45° in the present study. Additional H_2 gas can be supplied from pipes attached to the vicinity of the inlet of the D-module. The gas pipes are connected to a piezoelectric valve and a small gas tank installed outside of the chamber of GAMMA 10/PDX. The amount of gas supply can be controlled by changing the plenum pressure (i.e., pressure in the tank), as well as the timing and duration regarding the opening of the piezoelectric valve. At the back side of the D-module, an exhaust port with a door covering the port (exhaust door) is installed. When the exhaust door is open, neutral particles are drained to the outside of the D-module through the port and then pumped at the cryopumps in the end region [20].

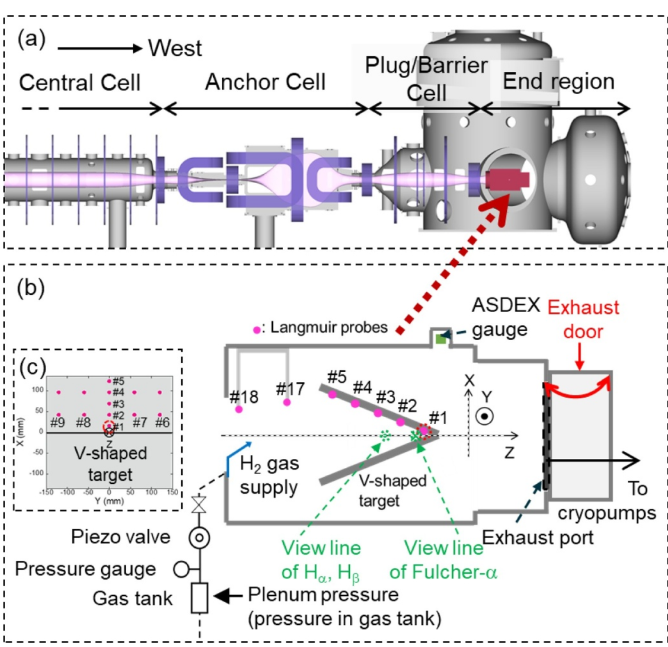

Fig. 1. Schematic view of (a) half body of GAMMA 10/PDX, (b) divertor simulation experimental module (D-module), and (c) V-shaped target in the D-module.

Thirteen Langmuir probes (LPs) are installed on the upper target, as shown in Fig. 1(c), and two LPs are installed near the inlet of the D-module, as indicated in Fig. 1(b). These LPs are numbered as shown in Fig. 1(b) and (c). LPs #1–5, #17, and #18 are installed at the same Y position ($Y = 0$) to measure the parameter distributions toward the Z-axis. LPs #2 and #6–9 are installed at the same X and Z positions to measure the distributions along the Y-axis. The H_α and H_β line emissions and Fulcher-α band emissions of H_2 in the D-module can be measured using spectrometers with sightlines, as shown in Fig. 1(b). The neutral pressure in the D-module is measured using an ASDEX type fast ion gauge mounted at the top side of the D-module.

3. Results and discussion

3.1. Experiment overview

Plasma was produced for 400 ms using ion cyclotron range of frequency (ICRF) heating. Additional H_2 gas was supplied to the divertor simulation plasma for both cases when the exhaust door was both closed and fully open. The piezoelectric valve was opened from 10 ms after the beginning of the plasma production. The plenum pressure scan was conducted on a shot-by-shot basis. With the door closed, the H_2 gas was supplied at plenum pressures of 200, 400, 600, and 750 mbar. With the door open, the plenum pressures were 400, 800, 1000, and 1200 mbar. A higher H_2 plenum pressure was needed to decrease T_e to a value low enough to lead to detachment. Fig. 2 shows the time evolution of the (a) diamagnetism of plasma in the central cell, (b) electron line density in the west plug region, (c) total gas pressure in the D-module (P_n), (d) T_e, (e) n_e, and (f) ion saturation current (I_{is}) during typical discharges in which plasma detachment was observed with the door closed (shot #243476) and open (shot #243463). The plenum pressures with the door closed and open were 750 and 1200 mbar, respectively. The values of T_e, n_e, and I_{is} above were measured using LP #1 near the corner of the V-shaped target, as shown in Fig. 1(b) and (c). The value of n_e was evaluated using the electron saturation current. During a discharge, the diamagnetism of the central cell plasma did not change significantly, and the upstream electron line density in the west plug region increased over time. After a time t of ~400 ms, the upstream plasma of the D-module was nearly the same with the door closed as when it was open. Near the corner of the V-shaped target in the D-module, T_e monotonically decreased to ~2 eV. Both n_e and I_{is} first increased and then decreased, which is called rollover, indicating plasma detachment caused by MAR [17]. With the door open, a reduction of n_e and I_{is} after the rollover was smaller than that with the door closed.

Next, we focus on the spatial profiles of the plasma in the D-module. Fig. 3 shows profiles of (a) T_e, (b) n_e, and (c) I_{is} toward the Z-axis, which is averaged over t = 200–220 ms (shown in Fig. 2). The profiles with the exhaust door closed and open were almost the same. Fig. 3(d)–(f) show the same set of profiles as Fig. 3(a)–(c) averaged over t = 400–420 ms. Near the inlet of the D-module, the profiles in the two cases were almost the same. Near the target, the T_e profiles were also almost the same; however, n_e and I_{is} with the door open were higher than with the door closed. Fig. 4(a)–4(c) and 4(d)–4(f) show the profiles along the Y-axis near the corner averaged over t = 200–220 and

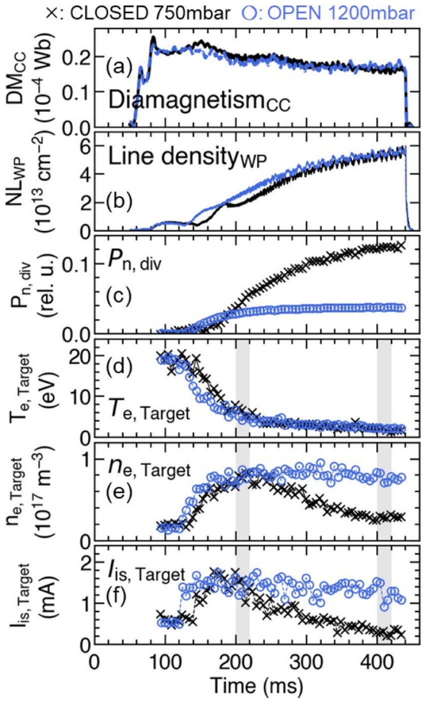

Fig. 2. Time evolution of the (a) diamagnetism of the central cell plasma, (b) electron line density of the west plug plasma, (c) total gas pressure in the D-module, (d) electron temperature, (e) density, and (f) ion saturation current. The ion saturation current, electron temperature, and density were measured using a Langmuir probe installed near the corner of the V-shaped target (LP #1), as shown in Fig. 1(b) and (c). Black ×, with the exhaust door closed; blue ○, with the door open. (For interpretation of the references to color in this figure legend, the reader is referred to the web version of this article.)

400–420 ms, respectively. Similarly, the profiles for both cases were almost the same during the former period; however, n_e and I_{is} with the door open were higher than those with the door closed during the latter period. The above results including the parameters in the central cell and the west plug region indicate that, from the upstream to the inlet of the D-module, the plasma in both cases were almost the same but there was a clear difference in the characteristics of the plasma detachment near the V-shaped target owing to the pump.

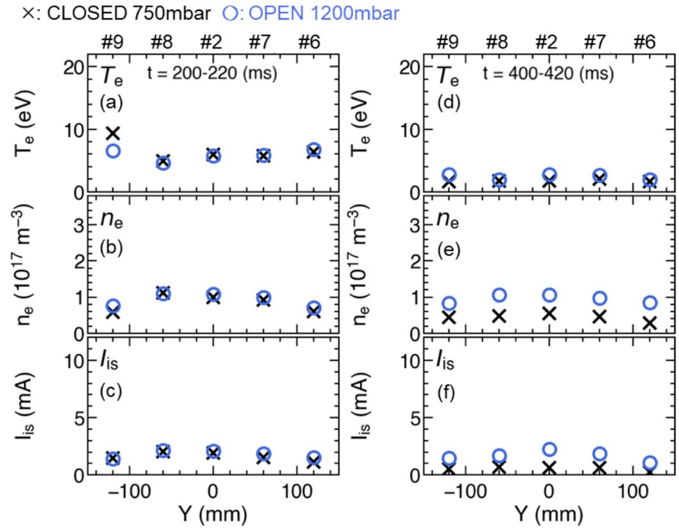

Fig. 4. Profiles of the (a) electron temperature, (b) electron density, (c) ion saturation current measured by probes #2 and #6–9 when the electron temperature near the corner was ∼5 eV (t = 200–220 ms in Fig. 2), and the distributions of the (d) electron temperature, (e) electron density, and (f) ion saturation current measured by the probes when the temperature was ∼2 eV (t = 400–220 ms in Fig. 2). Black ×, with the exhaust door closed; blue ○, with the door open.

3.2. Details of the observation near the corner of the V-shaped target

In this section, the differences in the characteristics of the detachment near the corner between the cases with the door closed and open are described. One of the important parameters for the reaction rate of the MAR leading to detachment is T_e. Fig. 5 shows the parameters of the plasma plotted against T_e as measured using LP #1 with data at the four respective plenum pressures mentioned in the previous section. As shown in Fig. 5(a) and 5(b), in both cases, I_{is} had a peak at a T_e of ∼10 eV and n_e had a peak at a T_e of ∼5 eV. When T_e was higher than or equal to the respective values, I_{is} and n_e in both cases were almost the same at each value of T_e. However, when T_e decreased from the respective values, the decreases in I_{is} and n_e with the door open were smaller than those with the door closed. In addition, within the T_e range, the intensity ratio of H_α to H_β ($I_{H\alpha}/I_{H\beta}$) with the door open was lower than that with the door closed, as shown in Fig. 5(c)–5(e). The MAR processes are divided into three chains of reactions, as shown in

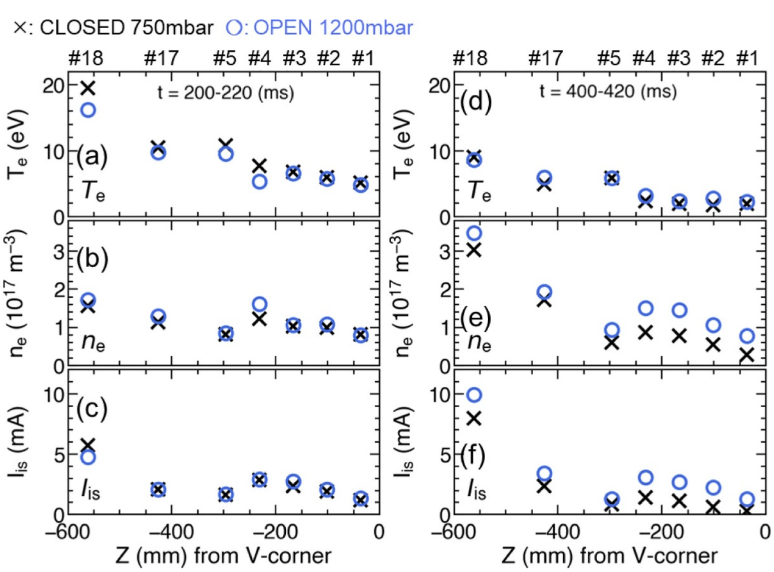

Fig. 3. Profiles of (a) electron temperature, (b) electron density, (c) ion saturation current measured by probes #1–5, #17, #18 when the electron temperature near the corner was ∼5 eV (t = 200–220 ms in Fig. 2), and distributions of (d) electron temperature, (e) electron density, and (f) ion saturation current measured by the probes when the temperature was ∼2 eV (t = 400–220 ms in Fig. 2). Black ×, with the exhaust door closed; blue ○, with the door open.

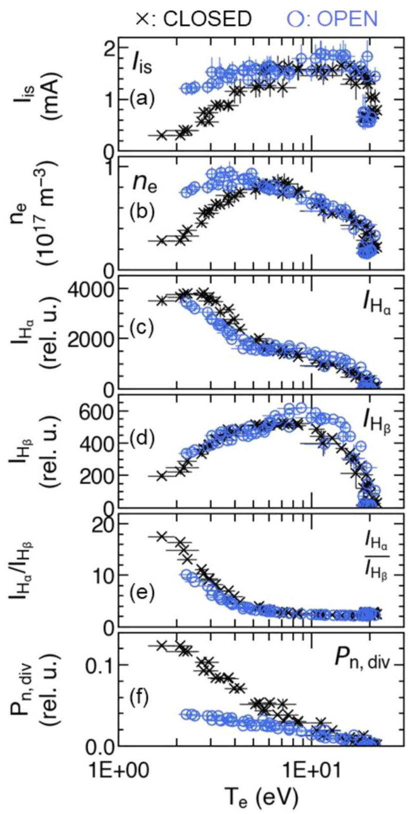

Fig. 5. (a) Ion saturation current, (b) electron density, (c) intensity of H_α line, (d) H_β line, (e) intensity ratio of H_α to H_β, and (f) total gas pressure plotted against the electron temperature. Black ×, with the exhaust door closed; blue ○, with the door open.

Table 1
Reaction processes of MAR.

• DA-MAR	·DA	$H_2(v) + e \rightarrow H^- + H$
	·MN	$H^- + H^+ \rightarrow H + H^*$
• IC-MAR	·IC	$H_2(v) + H^+ \rightarrow H_2^+(v) + H$
	·DR2	$H_2^+(v) + e \rightarrow H + H^*$
• MIC-MAR	·IC	$H_2(v) + H^+ \rightarrow H_2^+(v) + H$
	·MIC	$H_2(v) + H_2^+(v) \rightarrow H_3^+(v) + H$
	·DR3	$H_3^+(v) + e \rightarrow 3H, H_2(v) + H^*$

Table 1, namely, DA-MAR, IC-MAR, and MIC-MAR. In DA-MAR, the DA reaction is followed by an MN reaction. In IC-MAR, the atomic-to-molecular ion conversion (IC) is followed using a dissociative recombination (DR2). In MIC-MAR, the IC reaction is followed by the MIC reaction and two types of dissociative recombination (DR3). In the plasma detachment in GAMMA 10/PDX, DA-MAR (the source of H_α) is promoted by MIC-MAR, IC-MAR (the source of H_α and H_β) is impeded by MIC-MAR, and $I_{H\alpha}/I_{H\beta}$ increases with a decrease in n_e [17]. Therefore, in this study, the LP data and Balmer lines indicate that the total MAR reaction rate with the door open is lower than that with the door closed at the same T_e after the rollover. Next, to discuss the reason for the difference in the MAR reaction rate, we focus on hydrogen molecule parameters, namely, the rovibrational states of H_2 and the H_2 density (n_{H2}). These H_2 states and density affect the reaction rates of the DA, IC, and MIC reactions. The values of P_n in both cases were different, as shown in

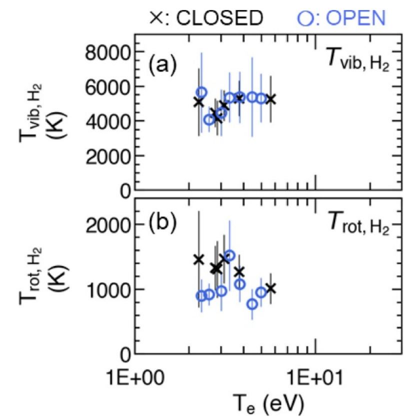

Fig. 6. (a) Vibrational temperature and (b) rotational temperature of hydrogen molecules estimated from Fulcher-α band spectra plotted against electron temperature. Black ×, with the exhaust door closed; blue ○, with the door open.

Fig. 5(f), indicating that the values of n_{H2} averaged over the entire region of the D-module were different; however, we discuss the local n_{H2} near the target plate later.

For the H_2 rovibrational states, based on the coronal model [21], we evaluated T_{vib} and T_{rot} of H_2 from the Fulcher–α band spectra and T_e measured using LP #1. Fig. 6 shows (a) T_{vib} and (b) T_{rot} plotted against a T_e of lower than ~6 eV. In this experiment, the fitting errors of T_{vib} and T_{rot} were large owing to the short exposure time of the spectrometer and resulting low S/N ratio. To improve the S/N ratio and the errors by summing up the spectra, additional experiments were conducted. Based on Fig. 6 and the additional data, it was confirmed that T_{vib} and T_{rot} in cases with the door closed and open were almost the same at each T_e, indicating that the rate coefficients of the DA reaction in both cases were almost the same.

For n_{H2}, we evaluated n_{H2} near the corner of the V-shaped target using the intensities of the Fulcher–α band spectral lines and n_e. Based on the coronal model, when the values of T_e, T_{vib}, and T_{rot} are constants, the intensities are proportional to $n_{H2} \times n_e$. Because T_{vib} and T_{rot} in both cases were almost the same at each T_e, the intensity can be used as an indicator of $n_{H2} \times n_e$. Fig. 7 shows the intensity of the Q1 branch ($v = v' = 0$) (I_{Q1}) and I_{Q1} normalized by n_e (I_{Q1}/n_e, as an indicator of n_{H2}), where v and v' indicate the vibrational levels of the upper and lower states during the transition, respectively. The I_{Q1} values in both cases were almost the same at each T_e, indicating that the values of

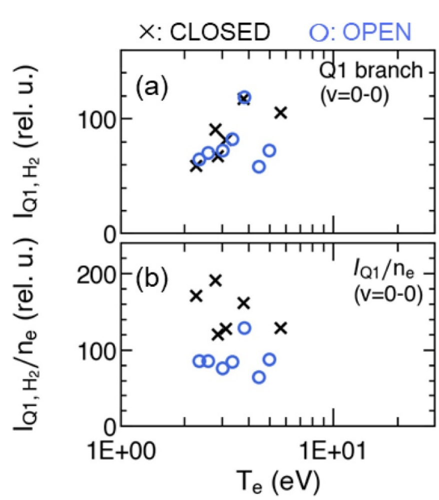

Fig. 7. (a) Intensity of Q1 branch (v = v' = 0) of Fulcher-α band spectra and (b) Q1 branch intensity normalized by electron density. Black ×, with the exhaust door closed; blue ○, with the door open.

$n_{H2} \times n_e$ were also nearly the same. In addition to the results of T_{vib} and T_{rot}, the DA reaction rates with the door closed and open were suggested to be almost the same. However, I_{Q1}/n_e with the door open was lower than that with the door closed, indicating that n_{H2} near the corner with the door open was lower. This also suggests that T_e can be decreased even with a lower n_{H2} when the exhaust door is open. The above results suggest that the total MAR reaction rate with the door open was lower than that with the door closed owing to the low n_{H2}, among other reasons.

For a more detailed analysis regarding whether the difference in only n_{H2} can cause a difference in the MAR reaction rate, it is important to investigate the reaction rates of individual processes in the MAR by measuring the densities of the ions, such as H^-, $H_2{}^+$, and $H_3{}^+$, using a mass spectrometer and/or by solving the rate equations including the lifetime of the ion species. In addition to the n_{H2} effect, it is also important to investigate the effect of T_i because T_i affects the rate coefficients of the MN and IC reactions. However, this is left for a future study.

4. Summary

The aim of this study was to determine the effects of the rovibrational states of H_2, n_{H2}, and T_e on the plasma detachment caused by MAR. An experiment was conducted to change these parameters by combining the H_2 gas puff and a pump from the D-module through the exhaust door in the GAMMA 10/PDX tandem mirror. The additional gas was supplied to the divertor simulation plasma with the exhaust door both closed and open. With the door open, the gas was supplied at a higher plenum pressure than that with the door closed, decreasing T_e near the target plate to almost the same value as that with the door closed. In both cases, with a decrease in T_e, rollover of n_e and I_{is} was observed. After the rollover, decreases in n_e and I_{is} along with T_e when the door was open were smaller than when the door was closed. The intensity ratio $I_{H\alpha}/I_{H\beta}$ with the door open was lower than that with the door closed at the same T_e. These indicate that the total reaction rate of the MAR leading to plasma detachment with the exhaust door open is lower than that with the door closed at the same T_e after the rollover. The values of T_{vib} and T_{rot} of H_2 in both cases were almost the same at each T_e. By contrast, n_{H2} with the door open was lower than that with the door closed, indicating that T_e can decrease even with a lower n_{H2} when the exhaust door is open. The above results suggest that the MAR reaction rate with the door open was lower than that with the door closed owing to the low n_{H2}, among other reasons.

Declaration of Competing Interest

The authors declare that they have no known competing financial interests or personal relationships that could have appeared to influence the work reported in this paper.

Acknowledgments

The authors would like to thank the members of the GAMMA 10 group at the University of Tsukuba for their support with the experiments. This study was conducted with the support of the NIFS Collaborative Research Program (NIFS16KUGM119).

References

[1] G.F. Matthews, J. Nucl. Mater. 220–222 (1995) 104.
[2] S.I. Krasheninnikov, et al., Phys. Plasmas 23 (2016) 055602.
[3] S.I. Krasheninnikov, et al., J. Plasma Phys. 83 (2017) 155830501.
[4] A.W. Leonard, Plasma Phys. Control. Fusion 60 (2018) 044001.
[5] C. Kurz, et al., Plasma Phys. Control. Fusion 39 (1997) 963.
[6] S.I. Krasheninnikov, et al., Phys. Lett. A 214 (1996) 285.
[7] A.Yu. Pigarov, et al., Phys. Lett. A 222 (1996) 251.
[8] N. Ohno, et al., Plasma Phys. Control. Fusion 59 (2017) 034007.
[9] N. Ohno, et al., Phys. Rev. Lett. 81 (1998) 818.
[10] A. Tonegawa, et al., J. Nucl. Mater. 313-316 (2003) 1046.
[11] E.M. Hollmann, et al., Rev. Sci. Instrum. 72 (2001) 623.
[12] R.K. Janev, et al., Collision Processes in Low-Temperature Hydrogen Plasmas, (2003), p. 4105 FZ-Juelich Report.
[13] K. Sawada, et al., Atoms 4 (4) (2016) 31.
[14] K. Miyamoto, et al., J. Nucl. Mater. 313-316 (2003) 1036.
[15] Y. Nakashima, et al., Nucl. Fusion 57 (2017) 116033.
[16] Y. Nakashima, et al., Fusion. Sci. Technol. 68 (2015) 28.
[17] M. Sakamoto, et al., Nucl. Mater. Energy 12 (2017) 1004.
[18] A. Terakado, et al., AIP Conf. Proc. 1771 (2016) 050008.
[19] K. Nojiri, et al., AIP Conf. Proc. 1771 (2016) 060008.
[20] Y. Nakashima, et al., Vacuum 41 (1990) 1561.
[21] B. Xiao, et al., Plasma Phys. Control. Fusion 46 (2004) 653.